CHEMISTRY OF MATERIALS

pubs.acs.org/cm

Article

Enabling Narrow Emission Line Widths in Colloidal Nanocrystals through Coalescence Growth

James Cassidy, Cole Ellison, Jacob Bettinger, Mingrui Yang, Pavel Moroz, and Mikhail Zamkov*

Cite This: *Chem. Mater.* 2020, 32, 7524–7534

Read Online

ACCESS | Metrics & More | Article Recommendations | Supporting Information

ABSTRACT: With continuing progress in the chemical synthesis of colloidal semiconductor nanocrystals (NC), one property that remains elusive to the rational design is the ensemble photoluminescence (PL) line width. Given the growing demand for NC-based light-emitting materials, substantial research effort has been dedicated to this issue. Here, we demonstrate a postsynthetic strategy that allows reducing emission line widths of CdSe and CdS NCs to near single-particle levels while enhancing the PL quantum yield. The key idea behind the synthetic approach lies in employing a nonclassical coalescence growth mechanism, which leads to size focusing irrespective of the initial sample morphology. Numerical simulations accurately predict the observed particle size evolution, confirming the ability of coalescence growth to promote size focusing of semiconductor colloids. Ultimately, we expect that the demonstrated coalescence growth strategy could enable a rational control of nanocrystal size distributions and corresponding spectral line widths in many types of semiconductor NCs.

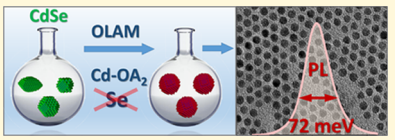

INTRODUCTION

Colloidal semiconductor nanocrystals (NCs) have become an attractive material platform for the solution processing of optoelectronic devices.[1] The ability to tune NC emission and absorption characteristics via the particle size has enabled new paradigms in solid-state lighting,[2−11] sensing,[12−16] and energy harvesting.[17−22] At present, one of the challenges facing the development of NC technologies concerns the reduction of the particle size dispersion toward improving ensemble spectral characteristics.[23] This issue has been intensely investigated over the years[23−35,44] and continues to represent one of the main synthetic challenges of the colloidal NC research.[36−43]

Most traditional strategies for size focusing of colloidal NCs rely on controlling the precursor conversion rates during growth. The basic idea behind these methods follows the Sugimoto principle[44,45] stating that nanocrystals smaller than a certain critical size (r^*) dissolve, while larger ones grow (Figure 1a, blue curve). Under these conditions, size focusing can be achieved through secondary precursor injections (or a delayed precursor decomposition), which lower the critical size, r^*, to just below the average size of particles present in the solution. This causes most nanoparticles to exhibit a positive growth rate, $dr/dt > 0$, with a corresponding size dependence that eventually results in narrowing of the particle size distribution.

In addition to the classical, precursor-controlled synthesis, some reports[46−56] have demonstrated the existence of a fundamentally different growth mechanism, which involves the coalescence of already preformed nanoparticles in the reaction mixture. This process is recognized as an important mechanism contributing to the formation of metal nanoparticles[57−60] and is believed to play a significant role in the size evolution of semiconductor NCs. In the low-temperature regime, the coalescence (aggregative) growth of semiconductor NCs is known to cause oriented attachment (OA)[61,62] of nanoparticles along matching crystallographic directions. The OA strategy has been widely explored for fabricating two-dimensional (2D) nanoplatelets[63,64] and nanoribbons[65−67] via cluster aggregation. The less explored, high-temperature coalescence regime, on the other hand, allows nanoparticles to aggregate along random crystallographic orientations, producing larger, spherically shaped colloids. An example of this process is illustrated in Figure 1b, where the coalescence of 5 nm CdS NCs in ligand-saturated solutions ([oleylamine] >60%) leads to a 3.5-fold increase in the average particle size despite the absence of precursors in the mixture. Notably, the final product appears to be monodisperse. The driving force behind the coalescence-induced size focusing is the $\sim 1/R$ dependence of the nanocrystals growth rate (dr/dt) on the particle size (see Figure 1a, red curve). Under these conditions, smaller particles grow faster than larger ones for any r, leading to eventual focusing of particle sizes. This contrasts the traditional, precursor conversion strategy, which requires $r > r^*$ for size focusing. It is, therefore, reasonable to expect that coalescence growth conditions could represent a more effective strategy for reducing the size dispersion of semiconductor NCs as compared to the classical precursor-controlled synthesis.[47,55]

Received: July 9, 2020
Revised: August 6, 2020
Published: August 7, 2020

https://dx.doi.org/10.1021/acs.chemmater.0c02874
Chem. Mater. 2020, 32, 7524–7534

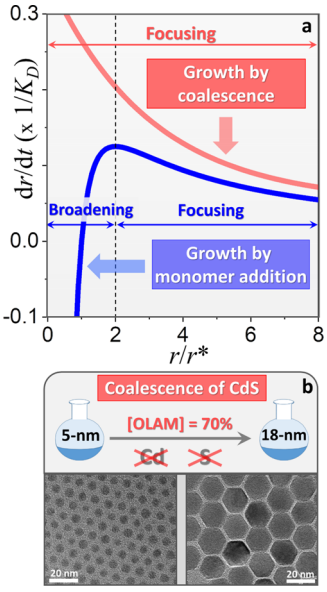

Figure 1. (a) Traditional and coalescence-based growth models. The blue curve shows the particle size dependence of the NC growth rate (dr/dt) for the classical, monomer-addition-based mechanism,[44] while the red curve shows an expected size-dependent rate for the coalescence growth mechanism, calculated using the diffusive-aggregation model (see the Supporting Information section). The monomer addition growth model exhibits both positive ($r > r^*$) and negative ($r < r^*$) growth regions, which could promote either focusing or defocusing (Ostwald ripening)[68] of the size distribution. Meanwhile, the rate of the coalescence growth is always positive and is inversely proportional to r, which leads to unconditional size focusing of particle populations. The parameter K_D is a rate constant as indicated in Figure SF1. (b) Illustration of the coalescence growth of CdS NCs. The diameter of CdS nanoparticles increased more than 3-fold upon heating to 240 °C in the reaction mixture containing free ligands (OLAM—70% by volume). No precursors are introduced during the reaction. A portion of Figure 1b was adapted with permission from ref 50. Copyright 2018 American Chemical Society.

Here, we report on the synthesis of colloidal CdSe NCs exhibiting spectrally narrow emission with corresponding line widths approaching single-particle values. The synthetic innovation lies in the employment of coalescence-only growth conditions enabled by high concentrations of L- and Z-type ligands in the reaction mixture. The presence of more than 60% L-type ligand promotes the coalescence of NCs, while the presence of approximately 2% by volume of Z-ligand inhibits the traditionally oriented attachment mechanism, thus allowing for the formation of spherical NCs. When applied as a postsynthetic treatment, this strategy results in a reproducible reduction of the particle size dispersion, enabling CdSe NC photoluminescence with full width at half-maximum (FHWM) of as low as 72 meV and quantum yield above 20% without shelling. Model calculations based on the diffusive-aggregation approach[69] accurately predict the particle size evolution observed for CdSe NCs, indicating that coalescence growth can lead to unconditional focusing of particle sizes irrespective of the initial sample morphology. This premise was confirmed through the application of the coalescence growth strategy to a number of polydisperse CdSe NC samples as well as samples of CdS semiconductor NCs, where an apparent reduction of the emission line width was observed as well. Overall, present experimental findings backed by theoretical calculations indicate that ligand-controlled coalescence growth could represent an attractive postsynthetic strategy for size focusing of many types of semiconductor NCs.

RESULTS AND DISCUSSION

The traditional approach to the colloidal synthesis of semiconductor nanocrystals relies on a controlled addition of monomers released during the thermal precursor decomposition. This process is characterized by the Gibbs−Thomson equation,[70] which balances the reduction of free energy due to monomer-to-nanoparticle bonding with the increase of the surface energy resulting from such an addition.[71−77] The interplay of the positive and negative energy terms in the Gibbs−Thomson equation gives rise to the well-known Sugimoto principle[44] formulating that nanocrystals greater than a certain critical size exhibit a positive growth rate (Figure 1a, blue curve and Figure SF1) while those that are smaller dissolve. Consequently, if nanoparticle sizes are distributed on both sides of the critical radius (r^*), the particle size dispersion would naturally increase with the reaction time (Oswald ripening[68]). With additional precursor injections at the growth temperature, however, one can shift the critical nanocrystal size to a smaller value causing the majority of nanocrystals in the solution to exhibit a positive growth rate. Under these conditions, smaller nanocrystals in the distribution will grow faster than the larger ones, leading to size focusing.

When large proportions of free ligands are present in the reaction mixture, the contribution of coalescence processes into the particle growth becomes significant.[50] At low-reaction temperatures, such aggregative processes primarily lead to the oriented attachment of nanocrystals,[78] which represents a well-known strategy for the synthesis of nanoplatelets and nanoribbons,[63,65] nanorods,[62] and other, more complex morphologies.[79,80] For instance, CdSe nanoplatelets are known to form through the oriented attachment of magic size clusters (e.g., $CdSe_{13}$, $CdSe_{34}$)[81,82] in the presence of cadmium carboxylate (Z-type ligand), while PbS nanosheets[83] are synthesized by the oriented attachment of <3 nm nanocrystals in the presence of chloride compounds. The decrease of the surface energy through the decrease of the number of unsatisfied surface bonds has been identified as the driving force for the attachment of these NCs to form a new particle morphology.[84]

When free ligands are introduced at temperatures exceeding a certain thermal threshold (e.g., 220−240 °C for cadmium chalcogenides), attachment of the two nanoparticles can occur along random crystallographic directions.[85] This is usually followed by the self-reorganization of coalesced structures into spherically shaped, larger nanoparticles (see Figure 1b).[86−88] Previous studies[50,88−90] have shown that the growth rate associated with the coalescence mechanism is positive and approximately proportional to $1/r$ (Figure 1a, red curve), which leads to size focusing regardless of the nanoparticle size.[30,46,50,52,53,55] This trend contrasts the classical monomer-addition growth, where size focusing is observed only for $r > r^*$ (Figure 1b, blue curve). The experimental evidence in favor of a positive coalescence growth rate, dr/dt, has been provided by a recent report[50] investigating an aggregative growth of mixed nanoparticle samples containing small- and large-diameter CdS NCs (Figure SF6a−f). Upon heating of this mixture in ligand-saturated solutions to above the coalescence threshold, absorption features of both small and large nanoparticles were observed to red-shift,[50] indicating that dr/dt was positive

https://dx.doi.org/10.1021/acs.chemmater.0c02874
Chem. Mater. 2020, 32, 7524−7534

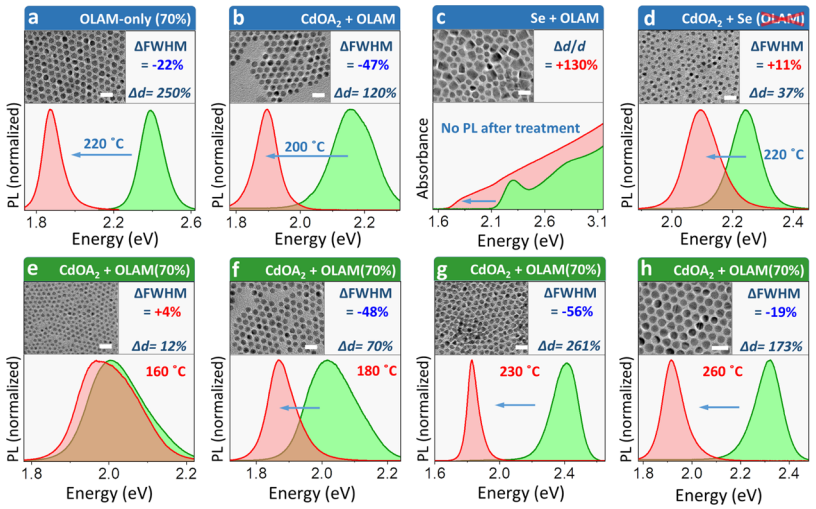

Figure 2. Results of several characteristic growth reactions (60−90 min in duration) showing the size evolution of small-diameter CdSe NCs (initial PL shown in green) in the presence of free ligands (OLAM) and coprecursors ($Cd(OA)_2$ and Se). (a) OLAM-alone treatment (no precursors) causing a significant increase in the average particle size (Δd = 250% for the displayed reaction) and moderate size focusing (ΔFWHM = −22%). (b) Postsynthetic treatment involving a combination of OLAM (70% by volume) and the Z-type ligand ($Cd(OA)_2$, no Se) resulting in the increase of the average particle size (Δd = 120%) accompanied by size focusing (ΔFWHM = −47%). (c) Treatment involving a combination of OLAM (70% by volume) and Se (no $Cd(OA)_2$) resulting in a rapid particle growth and significant broadening of the particle size distribution ($\Delta d/d$ = +130%). The band gap emission was quenched. (d). Growth by monomer addition (no OLAM, $Cd(OA)_2$/Se = 3:1) producing a moderate increase in the particle size (Δd = 37%) and slight broadening of the particle size dispersion (ΔFWHM = +11%). (e−h) Investigating the effect of the reaction temperature during the postsynthetic treatment in a mixture of OLAM (70%) and $CdOA_2$ (no Se precursor). (e) T = 160 °C. (f) T = 180 °C. (g) T = 230 °C. (h) T = 260 °C.

for all particle diameters. Notably, smaller-size intermediates have not been detected during the reaction.

To understand the interplay between the classical precursor-conversion and coalescence-driven growth mechanisms, we first looked into the evolution of CdSe NCs in the presence of free ligands only (no precursors). To this end, small-diameter CdSe NCs (d = 2.5−4 nm)[91,92] were loaded into a flask containing a 70:30 oleylamine (OLAM)/octadecene (ODE) mixture by volume and subsequently heated to 230−240 °C. Please see Table ST1 for the summary of all of the performed synthetic experiments. After 60−90 min of exposure, the average particle diameter increased by 150−250% (see a representative PL spectrum of CdSe NCs before and after the reaction in Figure 2a). The growth was assumed to undergo entirely by interparticle coalescence since no precursors were added during this treatment. The coalescence growth was also evident by the character of the PL evolution in Figure SF2, where a gradual reduction of the PL line width suggested that smaller particles indeed grew faster than the larger ones (as expected due to the inverse size dependence of the particle growth rate in Figure 1a, red curve). In fact, for all of the attempted 70:30 OLAM/ODE treatments, a gradual reduction of the particle size dispersion was observed (ΔFWHM between −20 and −40%), consistent with previous reports.[50,53,55] We note that a monotonous decrease in the PL FWHM indicates minimal contributions from Ostwald ripening, as the latter growth mechanism inevitably broadens the emission line width at intermediate reaction stages due to the dissolution of smaller particles in favor of larger ones (when $r/r^* < 2$ in Figure 1a).

Interesting growth dynamics were observed when only one of the two precursors, either $Cd(OA)_2$ or Se, was added to the OLAM/ODE reaction mixture. Under these conditions, particle growth can proceed only via the coalescence mechanism since the monomer-addition growth requires both precursors to be present. Remarkably, the growth dynamics in the presence of either Cd or Se were noticeably different in comparison with that of OLAM-only reactions. For instance, when $Cd(OA)_2$ Z-type ligand was present in the OLAM/ODE mixture, the CdSe particle size dispersion has decreased significantly (Figure 2b,f−h) with the final emission line width being narrower than in the case of the OLAM-alone treatment. Notably, focusing of CdSe NCs was observed only when the reaction temperature exceeded the T = 180 °C thermal threshold (Figure 2e−h), which was consistent with the coalescence-driven growth mechanism. When the Se precursor was introduced in the OLAM/ODE mixture, the postsynthetic treatment resulted in a significant increase of the particle size dispersion marked by a large variety of shapes and sizes in the final product (transmission electron microscopy (TEM) image in Figure 2c). The rate of particle coalescence under the (Se + OLAM) growth conditions appeared to be even faster than in the case of ($Cd(OA)_2$ + OLAM) mixture, as could be attested by the Δd = +310% increase in the average particle size accompanying the +130% growth in the particle size dispersion ($\Delta d/d$).

For the next step, the size focusing treatment was performed using a combination of free ligands (OLAM/ODE = 70:30) and precursors ($Cd(OA)_2$ and Se). This environment permits both coalescence and monomer addition-based growth mechanisms to contribute to the evolution of CdSe NC sizes. According to several existing models that consider aggregative growth of nanoparticles in the presence of precursors,[59,89,93,94] a combination of the coalescence and monomer-addition processes could represent an efficient size focusing strategy. In the present experiments, we observed that the Cd to Se precursor ratio played an important role in the particle size evolution (Figure 3a). For instance, when Cd/Se > 2, the particle size dispersion was noticeably reduced with an overall reduction in the FWHM value exceeding that of OLAM

https://dx.doi.org/10.1021/acs.chemmater.0c02874
Chem. Mater. 2020, 32, 7524−7534

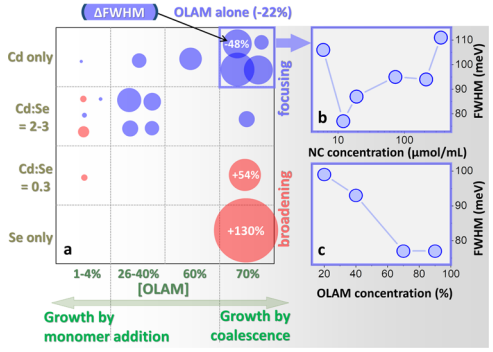

Figure 3. (a) Summary of coalescence growth reactions applied to small-diameter CdSe NCs. The concentration of a free ligand (OLAM) is plotted along the horizontal axis, and the varying precursor ratio, $Cd(OA)_2$/Se is plotted along the vertical axis. Overall, size focusing conditions (negative ΔFWHM expressed as the diameter of a blue circle) were enhanced at higher concentrations of OLAM due to an increased coalescence contribution to the growth. The presence of $Cd(OA)_2$ (without Se) was found to be necessary for further reduction of the particle size dispersion. Conversely, reactions containing low Cd/Se precursor ratios (<1) resulted in the broadening of the particle size dispersion, irrespective of OLAM concentrations. (b) Effect of the CdSe NC concentration (μmol/L) in the $Cd(OA)_2$ + OLAM (70%) growth mixture on the ultimate emission line width in the final product (FWHM). The initial line width of the starting CdSe NC samples was in the 105−174 meV range (see Table ST1). (c) Effect of OLAM concentration (%) in the $Cd(OA)_2$ + OLAM growth mixture on the ultimate emission line width of larger CdSe NCs (FWHM).

alone. In particular, coinjecting Cd and Se precursors at a ratio of 3:1 in the presence of OLAM has resulted in CdSe NCs with the emission line width of 87 meV. When the ratio of Cd to Se precursors was below 1, the growth dynamics have changed significantly from that of Cd-rich reactions. For instance, a OLAM/ODE = 70:30 mixture containing a Cd/Se = 1:3 precursor ratio resulted in the fast particle growth accompanied by a significant broadening of the particle size distribution. According to Figure 3a, ΔFWHM for this case was +60%. When only Se was injected (Cd/Se = 0) in the presence of OLAM (70%), the particle size dispersion in the final product broadened by +130% (Figure 2c), accompanied by full quenching of the band gap emission. The lack of PL in Se-treated CdSe NCs could be explained by the fact that in the absence of electronic doping, Se 2c orbitals will be occupied and can serve as hole traps. This is consistent with experimental observations of the hole-trapping limit to the PL QY in CdSe NCs following the displacement of cadmium carboxylate.[95] Density functional theory (DFT) theory developed for smaller NC models also predicted that two-coordinated Se atoms could introduce a midgap state in the band gap of the material.[96]

Size focusing dynamics under OLAM-deprived reaction conditions was investigated next. Only a minimal amount of OLAM (3−4%) needed to dissolve the Se precursor was present in the flask (see Table ST1 for the summary of all performed postsynthetic treatments). In this environment, the rate of the coalescence growth becomes sufficiently low to allow for the conventional, monomer-addition mechanism to become the primary process contributing to the nanoparticle size evolution. According to Figure 2d, under these conditions, the rate of nanoparticle growth was substantially lower than in the case of a coalescence-driven synthesis ($\Delta d/\Delta t$ (70% OLAM) = 150−250%/h; $\Delta d/\Delta t$ (4% OLAM) = 37%/h). Furthermore, the presence of both precursors (Cd and Se) was required for observing any changes in the particle diameter, which was consistent with the lack of coalescence contribution to growth. Introducing both precursors at a ratio of Cd/Se = 3:1 (Figure 2d) produced rather small changes in the average particle size. In this case, three separate experiments have resulted in a narrow distribution of ΔFMHW outcomes (ΔFWHM = −8% to +23%, Figure 3 and Table ST1), indicating that monomer addition-only growth conditions during a postsynthetic treatment are not likely to cause dramatic changes in the particle size dispersion.

Overall, the above experiments demonstrate that size focusing conditions are readily achieved when the coalescence contribution to particle growth is significant (high concentration of free ligands in the reaction mixture). In the absence of the coalescence growth, focusing of nanoparticle sizes was less reproducible (−8% < ΔFWHM < 23 %). The greatest reduction of the particle size dispersion (−48% < ΔFWHM < −20%) was observed in reactions containing Z-type ligands ($CdOA_2$) in combination with 60−70% OLAM (see Figure 2f,h). Both the concentration of nanoparticles in the reaction mixture (Figure 3b) and the percentage of OLAM in the flask (Figure 3c) played a role in determining the ultimate emission line width of treated NCs. It was observed that during the size focusing treatment, the initial concentration of CdSe NCs was reduced due to growth. For instance, for CdSe NCs with a first exciton peak at 520 nm and an initial concentration of 12 μmol/L (70 nmol total), the final concentration after coalescence growth was dropped to 0.3 μmol/L (1.2 nmol total). Notably, based on the number of moles and the average particle diameter, we estimate that the total volume for both the initial and final CdSe NC population was approximately the same.

We speculate that the presence of $Cd(OA)_2$ was necessary to facilitate inter- and intraparticle ion exchange processes necessary for size focusing and spherical nanocrystal morphologies. The second important role of the $Cd(OA)_2$ was its ability to suppress the oriented attachment of large-size CdSe NCs along the wurtzite *c*-axis, as discussed later in the text, which further helped reducing the particle size dispersion. Notably, a combination of $Cd(OA)_2$ and OLAM has helped improving the emission quantum yield of CdSe NCs, with the final product exhibiting QY over 20%. Such an improvement in the PL QY of OLAM-treated CdSe NC samples agrees with previous reports,[97−102] indicating an enhancement of the emission intensity (PL QY up to 50%)[103] upon binding of L-type ligands to undercoordinated surface Cd atoms. This interaction raises the energy of both the conduction and valence band edges toward vacuum,[104] which could effectively suppress hole trapping.

The demonstrated ability of coalescence processes to reduce the particle size dispersion represents a potentially useful strategy for lowering the ensemble PL line width to near single-particle levels. In general, the fundamental limit to the room-temperature emission line width for single CdSe NCs is determined by the lifetime of the excitation ($\sim h/\Delta\tau$), with further broadening being contributed by phonon coupling, exciton fine structure, and spectral dynamics.[105−108] Recently, Bawendi group[106] has reported the single-dot PL FWHM for CdSe NCs in the 60−75 meV range. Peng et al.[109] have studied the emission of magic size clusters observing an ultralow emission FWHM of 58−70 meV, with larger

https://dx.doi.org/10.1021/acs.chemmater.0c02874
Chem. Mater. 2020, 32, 7524−7534

structures exhibiting lower FWHM values. The ensemble PL peak width for conventional quantum dots produced by the state-of-art synthesis usually lies in the 90−150 meV range.[31,105,110] In general, ∼80−90 meV is considered as a narrow FWHM for ensemble PL of CdSe.[111]

To achieve near single-particle emission line widths, the coalescence growth was performed in the mixture of $Cd(OA)_2$ and OLAM free ligands ($Cd(OA)_2$/OLAM/ODE = 2:80:18 by volume). During a 60 min treatment, 3.1 nm CdSe NCs with an initial FWHM of ∼157 meV have gradually increased in size (Figure 4a) while exhibiting a progressively lower PL

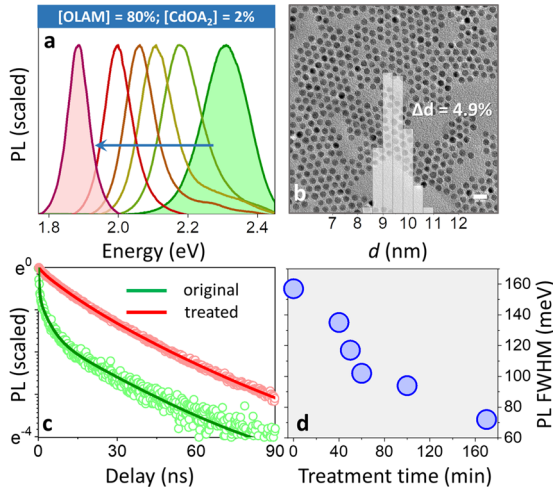

Figure 4. (a) Evolution of the CdSe NC PL spectra during size focusing in a mixture of OLAM (80%), $CdOA_2$ (2%), and ODE (18%). (b) TEM of CdSe NCs after the size focusing treatment. The standard size deviation is 9.5 ± 0.4 nm. The scale bar is 20 nm. (c) Changes in the PL intensity decay of CdSe NCs caused by the size focusing treatment. The PL lifetime of the final CdSe NC product is 27 ± 0.3 ns. (d) Evolution of the CdSe NC spectral line width (FWHM) during the size focusing treatment.

line width. The final product had an ensemble PL FWHM of 72 meV (Figure 4d) and the corresponding particle size dispersion of $\Delta d/d$ = 4.9% (based on TEM statistical analysis in Figure 4b). Several independent tests were performed on different batches of starting CdSe NCs (FWHM = 105−174 meV) all resulting in the final PL FWHM of 72−95 meV (see Table ST1). Notably, the observed line width was within 20% of a single-particle FWHM, reported in ref 107. In addition, the emission lifetime of treated nanocrystals was increased by almost an order of magnitude from its value in initial CdSe NC samples (Figure 4c).

To test whether the coalescence-growth approach represents an effective postsynthetic treatment for nanocrystals of other semiconductor materials, we have attempted size focusing of CdS NCs (Figure 5). To this end, 4.2 nm CdS colloids with an initial PL FWHM of 123 meV were loaded into a flask containing 64% of OLAM, 34% of ODE, and 2% of $Cd(OA)_2$. Upon heating the mixture to above the coalescence threshold temperature (T = 250 °C) for 95 min, we observed an increase in the average particle size accompanied by the reduction of the band gap emission FWHM from 123 to 92 meV. The ultimate size of CdS nanoparticles in the final product was estimated to be 8.1 nm (see Figure SF4).

The observed focusing of CdSe and CdS NC sizes is consistent with the existing theoretical literature on aggregative

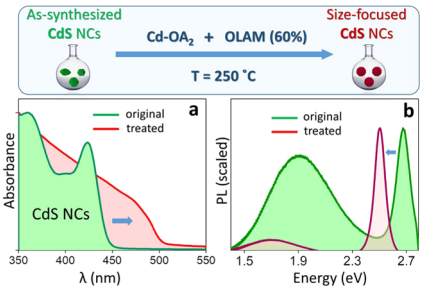

Figure 5. Size focusing of CdS NCs in a mixture of OLAM and $Cd(OA)_2$ free ligands. (a) Evolution of the absorption spectra after 60 min of reaction. The average particle size has increased from 4.2 to 8.1 nm. (b) Corresponding evolution of the emission spectra, showing the reduction in the band gap emission (ΔFWHM = −25%).

growth of colloidal nanoparticles.[59,89,93,94] For instance, early theoretical works have demonstrated that coalescence alone could be responsible for the formation of monodisperse nanoparticles of silica,[93] Au,[112] and silver.[94] Aggregative growth was also suggested as a possible mechanism for controlling the particle size distribution during NC synthesis.[59] Most of these studies have used the Smoluchowski rate equation[113] for modeling the kinetics of diffusion- or reaction-limited colloid aggregation.[114,115] Within this approach, the two primary particles, A_1, can aggregate upon collision resulting in the formation of secondary particles A_2, which in turn can further aggregate to form larger colloids, A_i. In general, the coalescence growth of any two particles A_i and A_j, each containing i and j numbers of primary particles, can be described as follows

$$A_i + A_j \xrightarrow{K_{ij}} A_k \tag{1}$$

where $A_k$represents a composite colloid containing k primary particles, such that $k = i + j$. The time-evolution of the A_k concentrations can be determined by solving the following rate equations

$$\frac{dN_k}{dt} = \frac{1}{2}\sum_{i+j=k} K_{ij}N_iN_j - N_k\sum_j K_{kj}N_j \tag{2}$$

where N_k is the concentration (number per unit volume) of A_k nanoparticle aggregates, and K_{ij} is the rate constants for the reaction between the i and j aggregates $K_{ij} = 4\pi(R_i + R_j)(D_i + D_j)$, where D is the diffusion coefficient (see the Supporting Information section for details).

The diffusion-limited aggregation (diffusive-aggregation) model outlined above assumes that collisions between nanoparticles are followed by their coalescence, regardless of the particle size. The experimental kinetics for cadmium chalcogenide NCs, however, shows that the coalescence growth does not occur for particles larger than a certain critical size ($dr/dt \to 0$ with increasing r, Figure 1a). This behavior agrees with the general premise of the viscoelastic collision theory of colloidal nanoparticles,[116] whose main principles follow the general framework of viscoelastic droplet coalescence. A simple model of droplet aggregation[117] suggests that during the coalescence of structured (crystallized) droplets, the interfacial energy of the two particles, $E_{interfacial}$, is reduced upon particle fusion, while the elastic energy, $E_{elastic}$, is increased by the compression of the internal structure. When the two processes balance each other ($E_{tot} = E_{interfacial} + E_{elastic}$

https://dx.doi.org/10.1021/acs.chemmater.0c02874
Chem. Mater. 2020, 32, 7524−7534

→ min), the coalescence process is arrested. In analogy to this model, we propose that as the two nanoparticles contact, coalescence is initiated when a ligand-based neck forms between them. The particles are then pulled together into a single spherical shape via the exchange of ions. This process is driven by the reduction of the interfacial energy, which in the case of two coalescing spheres is approximately exponential with the instantaneous geometric strain, $\varepsilon = \Delta L/(2 \times \text{init. particle diameter})$

$$E_{\text{interfacial}} = \gamma \times A(\varepsilon) = \gamma \times (A_0 + A_1 e^{-\varepsilon/A_2}) \quad (3)$$

where A is the total interfacial area of two coalescing particles and A_0, A_1, A_2 are the constants for the exponential decay fit.[117] Meanwhile, the strain energy of the two coalescing particles increases during the coalescence process. This is due to the two crystal lattices being compressed in a manner similar to the elastic compression of two springs. The energy term associated with the compression strain is given as

$$E_{\text{elastic}} = \frac{3}{2} G \varepsilon^2 V \quad (4)$$

where G is the particle shear modulus that characterizes the nanocrystal rigidity and V is the total volume of the coalescing nanostructures. The total energy of the two particles is thus given as a sum of the decreasing interfacial energy (eq 3) and increasing elastic energy (eq 4). The coalescence process is expected to stop when the total energy is minimized, $E_{\text{tot}}(\varepsilon) \rightarrow$ min. If the minimum of $E_{\text{tot}}(\varepsilon)$ is realized at a negligibly small strain ($\varepsilon < 0.02$), particle aggregation will not occur. Clearly, the final morphology of the two coalesced particles (full coalescence, particle coalescence, or no coalescence) depends on the value of the shear modulus, G. The temperature dependence of G follows the Mechanical Threshold Stress (MTS) model[118] for inorganic crystals, $G = G_0 - D/(\exp(T_m/T - 1))$, where G_0 is the shear modulus at $T = 0$ K and D is a material constant. When $T = T_m$, G diminishes, signifying the melting phase transition. According to Figure 6a, in the low-temperature regime ($T < T_m$), the elastic energy of the particles is too large for the total energy $E_{\text{tot}}(\varepsilon)$ to exhibit a minimum (red curve). Consequently, no coalescence is achieved (elastic stabilization). However, when $T > T_m$, the value of G drops abruptly with T, so that the total energy exhibits a decline with the increasing strain (green and blue curves). In this case, either a full or partial coalescence is achieved depending on the actual slope of the $G(T)$ curve. Notably, because the strain energy is directly proportional to the total volume, V, larger particles are less driven toward a full coalescence.

In the present work, the transition from viscose (aggregative) to viscoelastic (partly aggregative) collisions may occur even in the high-temperature regime, $T > T_m$ (220 °C), if the radii of fusing particles exceed a critical value $r = R_c$. This process is clearly manifested during the coalescence growth of CdS NCs in OLAM-only solutions (no $Cd(OA)_2$). According to Figures 6b and SF3a, once the critical size of CdS is reached, subsequent heating does not result in further coalescence. Instead, nanoparticles undergo oriented attachment along specific crystallographic directions, which causes the formation of nanorods (Figures 6b and SF3b). However, if $Cd(OA)_2$ is introduced along with OLAM, oriented attachment processes become suppressed and the average nanoparticle size does not increase above the critical size with further heating (Figure 6b). Along these lines, to model the

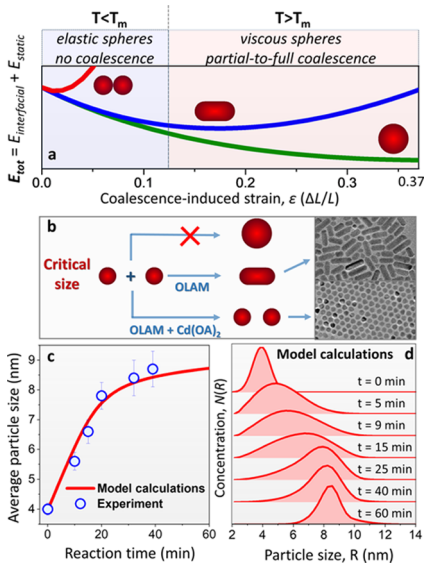

Figure 6. (a) Total energy of two spherical particles ($E_{\text{interfacial}} + E_{\text{elastic}}$) during coalescence. A zero strain, ε, corresponds to particles before coalescence and a maximum strain of 0.37 represents total coalescence into a spherical object. If the growth solution temperature, T, is lower than T_m, particles are too elastic to undergo coalescence (red curve). When $T > T_m$, either partial (blue) or full (green) coalescence is achieved. (b) Illustration of the critical size for particle coalescence, R_c. For $r > R_c$, the coalescence of randomly oriented nanocrystals becomes suppressed. In this case, subsequent heating can only resolve in the oriented attachment of large nanoparticles ($r = R_c$) along specific crystallographic directions (as usually observed in OLAM/ODE mixtures), which causes the formation of nanorods (see the TEM image in the insert). When $Cd(OA)_2$ is introduced into the OLAM/ODE reaction mixture, oriented attachment processes become inhibited causing the average nanoparticle size to remain spherical ($r = R_c$) despite further heating. (c) Diffusive-aggregation model calculations of the coalescence growth kinetics for CdSe NCs. The predicted temporal evolution of the particle size $r(t)$ (red curve) is compared with experimental data points (blue circles). The experimental error bars represent the uncertainty in the value of the average particle size due to an intrinsic uncertainty in the NC size-band gap scaling. (d) Model calculations of the particle size distribution during the coalescence growth.

effect of the critical size in this work, we assume that the coalescence rate (but not the collision rate, K_{ij}) approaches zero, if the size of A_k exceeds the critical size parameter, R_c.

Figure 6c,d illustrates the predictions of the diffusive-aggregation model for the evolution of the CdSe particle size. The initial rise of the theoretical $r(t)$ (red curve) indicates a fast coalescence growth at early times, which is followed by an asymptotic decrease of the growth rate when the average particle radius approaches the critical size, R_c. Similar $r(t)$ trends have been predicted for the aggregative growth of ZnS[119] and PbS[88] NCs within the Smoluchowski approach. In present calculations, the product of the initial particle concentration, N_1, and the primary particle diffusion coefficient, D_1, was designated as a fitting parameter to ensure a better match of theoretical parameters for solvent viscosity and particle number concentrations with that of an experiment.

According to Figure 6c, the calculated $r(t)$ accurately captures experimentally observed CdSe NC growth kinetics, evidenced by a gradual reduction of the growth rate with increasing particle size. Model calculations have also revealed an increase in the particle size dispersion at the early stages of

https://dx.doi.org/10.1021/acs.chemmater.0c02874
Chem. Mater. 2020, 32, 7524−7534

the reaction prior to size focusing (Figure 6d). To some degree, similar broadening in the experimental emission line width at early states of the postsynthetic treatment has been observed in several (but not all) tests (Figure SF5). This behavior could indicate that size focusing becomes more efficient when the average particle size approaches R_c. Indeed, when the starting particle diameter is several times lower than R_c, most of $A_i + A_j$ coalescence paths are still allowed, which causes a statistical broadening of the particle size distribution.

In summary, we demonstrate that nonclassical coalescence growth of cadmium chalcogenide NCs provides a robust strategy for controlling nanocrystal size distributions and corresponding spectral line widths. The demonstrated approach employs ligand-saturated solutions to stimulate the viscoelastic behavior of colloidal nanocrystals, during which elastic collisions between nanoparticles are followed by the viscous reorganization of surface ions, causing coalescence (aggregative) growth. Because the rate of the coalescence growth is inversely proportional to the particle size, size focusing is achieved irrespective of the initial sample morphology. In case of CdSe NCs, the coalescence growth resulted in monodisperse samples (Δd < 5%) exhibiting ensemble PL line widths near single-particle levels (FWHM = 72 meV). The final CdSe NC product exhibited enhanced PL lifetimes with the corresponding PL quantum yield above 20% (depending on the ultimate particle size). Numerical simulations based on the diffusive-aggregation model accurately predict the observed particle size evolution, confirming the ability of the coalescence growth to drive nanoparticle size focusing. Overall, we show that the coalescence growth strategy can produce high-quality chalcogenide nanocrystals needed for a wide range of applications. With future work, we expect this method to become potentially applicable to other semiconductor materials providing a general pathway for achieving the narrow spectral line widths.

METHODS

Materials. The following materials were used: cadmium oxide (CdO, 99% STREM), 1-octadecene (ODE, 90% Sigma-Aldrich), *n*-octadecylphosphonic acid (ODPA, PCI), octadecylamine (ODA, 90%, Acros), oleic acid (OA, 90% Sigma-Aldrich), sulfur (S, 99.99% Acros), Chloroform (anhydrous, 99% Sigma-Aldrich), oleylamine (OLAM, Tech., 70% Sigma-Aldrich), hexane (anhydrous, 95% Sigma-Aldrich), ethanol (anhydrous, 95% Sigma-Aldrich), tri-*n*-octylphosphine (TOP, 97% STREM), tri-*n*-octylphosphine oxide (TOPO, 99.0% Sigma-Aldrich), selenium powder (Se, 200 mesh, Acros), acetone (anhydrous, Amresco, ACS grade), stearic acid (97% Sigma-Aldrich), and tributylphosphine (TBP, 97% Sigma-Aldrich). All reactions were performed under argon atmosphere using the standard Schlenk technique. The VWR Clinical 100 centrifuge used for precipitation operated at 6500 rpm.

Synthesis of CdS NCs. CdS NCs were fabricated according to the previously reported procedure.[120] A mixture of 0.0768 g (0.6 mmol) of CdO, 3.6 mL of OA, and 24 mL of ODE in a 50 mL three-neck flask was heated to 240 °C until the solution turned optically clear and colorless. Then, the mixture was allowed to stir at this temperature at which point all of the sulfur precursor solution made by dissolving 0.02 g (0.625 mmol) of sulfur powder at 200 °C in ODE (10 mL) was quickly injected. The reaction was stopped by removing the flask from the heating mantle after 4−5 min. CdS NCs were separated from the solution by precipitating with methanol and redissolving the product in chloroform.

Synthesis of CdSe NCs. CdSe NCs were fabricated by adapting a previously reported procedure.[121] Briefly, TOPO (3.0 g), ODPA (0.025 g), OA (2.0 mL), and CdO (0.060 g) were mixed in a 50 mL flask, heated to 120 °C and exposed to vacuum for 1 h. Then, under argon, the solution was heated to 300 °C to dissolve CdO until the mixture turned optically clear and colorless. At this point, 1.5 g of TOP (that had been degassed at 120 °C for 30 min) was injected into the flask and the temperature was adjusted to 270 °C. The reaction flask with the Cd precursor was raised up from the heating mantle right before the injection of the Se precursor to get small-diameter nanoparticles. A selenium precursor prepared by dissolving 0.060 g of Se in 1 mL of TOP through heating to 150 °C under argon and cooling to room temperature was injected all at once into the raised flask (at 270 °C). The reaction temperature dropped to approximately 250 °C and was left stirring for 30 s before being quenched in a water bath, this yielded CdSe nanocrystals with a first exciton peak around 520 nm. After the synthesis, nanocrystals were precipitated with ethanol and washed by repeated redissolution in chloroform and precipitation with the addition of ethanol. Finally, the product was stored in chloroform (3 mL).

$Cd(OA)_2$ Stock Solution Synthesis. A 0.2 M $Cd(OA)_2$ stock solution was prepared by combining 15 mL of OA (47 mmol), 1.845 g of CdO (14 mmol), and 60 mL of ODE in a 100 mL three-neck round bottom flask. Under argon, the flask was heated to 240 °C until the solution turned clear. The final mixture was stored under argon and heated to 50 °C before being used.

Postsynthetic Treatment (Coalescence Growth). In a typical treatment, CdSe NCs, ODE, OLAM, and $Cd(OA)_2$ were degassed in a 25 mL round bottom flask at 80 °C for approximately 20 min. The flask was then switched over to argon using a Schlenk line, and the sample was heated to the desired temperature, typically 180−260 °C, for the remainder of the treatment. The concentration of NCs ranged 6−350 μmol/L, which was found to have a significant effect on the critical size and overall emission line width. To obtain monodisperse samples with approximately 72−80 meV PL line width, a 5 mL of solution of 12 μmol/L CdSe NCs (520 nm first absorption peak), with 70% by volume OLAM (4.2 mL), 0.6 mL of $Cd(OA)_2$ stock solution, and 1.2 mL of ODE, was degassed at 80 °C for 20 min; the mixture was then heated to 230 °C for 45−60 min before being quenched in a water bath.

Alternatively, narrow-line-width CdSe NCs could also be produced via coalescence of larger nanocrystals with a first absorbance peak at 577 nm and a concentration of 9 μmol/L (all other parameters were kept the same). When using solutions that were too concentrated, it was observed that the emission line width could not be reduced to below 90 meV.

To determine the concentration of our nanocrystal solutions, we used the work of Yu et al.[122] Briefly, for the less concentrated samples, the optical density of a small aliquot was placed into a cuvette and measured. Based on the first absorbance peak (size of the nanocrystal), the concentration could be calculated using the Beer−Lambert law. Alternatively, for the more concentrated samples, a small aliquot of the reaction mixture was diluted in chloroform and the optical density was then measured. The concentration was then calculated as above, but then the original concentration of the reaction mixture was determined via the dilution equation.

After the reaction mixture had cooled to room temperature, equal amounts of solution (approximately 3 mL) were placed in two 15 mL centrifuge tubes. To precipitate the product, 2 mL of chloroform and 6 mL of ethanol were added to each tube, which were then inverted several times and centrifuged for 5 min at 6500 rpm. The clear supernate was discarded and the remaining precipitate was dissolved in 2 mL of chloroform, 6 mL of ethanol was added, the centrifuge tubes were inverted several times, and then centrifuged 5 min at 6500 rpm. Finally, the precipitate was dissolved in hexane (5 mL) and centrifuged 30 s at 6500 rpm to remove any insoluble products. The final hexane solution was stored under ambient conditions and was stable for months.

Characterization. UV−vis absorption spectra were recorded using a CARY 60 scan spectrophotometer. High-resolution transmission electron microscopy (TEM) measurements were carried out using JEOL 311UHR operated at 300 kV and all other TEM images were acquired using a JEOL 2010F analytical electron microscope operating at 200 kV. Specimens were prepared by depositing a drop of

https://dx.doi.org/10.1021/acs.chemmater.0c02874
Chem. Mater. 2020, 32, 7524−7534

the NP solution in an organic solvent onto a carbon-coated copper grid and allowing it to dry in air. Powder X-ray diffraction (PXRD) measurements were carried out with a Bruker D8 Advance PXRD. Energy dispersive X-ray (EDX) analysis was performed using Hitachi 2700 operated at 20 kV. Emission spectra were acquired using a 405 nm PicoQuant PDL 800-D pulsed laser and measured with an Andor newton^{EM} SR-303i-A spectrograph. Time-resolved emission lifetime spectra were acquired using the same 405 nm pulsed laser, and photons were collected using ID Quantique's id100-50 single-photon detector and processed using a SPC-130 TCSPC module from Beckler & Hickl. Relative quantum yield measurements were acquired using a GS32 Intelite 532 nm CW DPSS laser (Cyanine3 NHS ester dye obtained from Lumiprobe was used as the reference).

■ ASSOCIATED CONTENT

Supporting Information

The Supporting Information is available free of charge at https://pubs.acs.org/doi/10.1021/acs.chemmater.0c02874.

Particle size dependence of the NC growth rate; evolution of the CdSe NC PL spectra; illustration of a critical size (R_c) for particle coalescence; TEM image of size focused, 8.1 nm CdS NCs; broadening of the particle size distribution; schematics of the aggregative growth process; summary of size focusing experiments (PDF)

■ AUTHOR INFORMATION

Corresponding Author

Mikhail Zamkov − *The Center for Photochemical Sciences, Department of Physics, and Department of Chemistry, Bowling Green State University, Bowling Green, Ohio 43403, United States;* orcid.org/0000-0002-8638-2972; Phone: 419-372-0264; Email: zamkovm@bgsu.edu; Fax: 419-372-9938

Authors

James Cassidy − *The Center for Photochemical Sciences and Department of Physics, Bowling Green State University, Bowling Green, Ohio 43403, United States*

Cole Ellison − *The Center for Photochemical Sciences and Department of Physics, Bowling Green State University, Bowling Green, Ohio 43403, United States*

Jacob Bettinger − *Department of Physics, Bowling Green State University, Bowling Green, Ohio 43403, United States*

Mingrui Yang − *The Center for Photochemical Sciences and Department of Physics, Bowling Green State University, Bowling Green, Ohio 43403, United States*

Pavel Moroz − *The Center for Photochemical Sciences and Department of Physics, Bowling Green State University, Bowling Green, Ohio 43403, United States*

Complete contact information is available at: https://pubs.acs.org/10.1021/acs.chemmater.0c02874

Notes

The authors declare no competing financial interest.

■ ACKNOWLEDGMENTS

This work was supported by the Award DE-SC0016872 (M.Z.) funded by the U.S. Department of Energy, Office of Science. J.C. was supported in part by NSF Award DMR-1710063. The authors acknowledge the financial support of the University of Michigan College of Engineering and NSF grant #DMR-9871177, and technical support from the Michigan Center for Materials Characterization.

■ REFERENCES

(1) Kovalenko, M. V.; Manna, L.; Cabot, A.; Hens, Z.; Talapin, D. V.; Kagan, C. R.; Klimov, V. I.; Rogach, A. L.; Reiss, P.; Milliron, D. J.; Guyot-Sionnnest, P.; Konstantatos, G.; Parak, W. J.; Hyeon, T.; Korgel, B. A.; Murray, C. B.; Heiss, W. Prospects of nanoscience with nanocrystals. *ACS Nano* **2015**, *9*, 1012−1057.

(2) Coe, S.; Woo, W. K.; Bawendi, M.; Bulovic, V. Electroluminescence from single monolayers of nanocrystals in molecular organic devices. *Nature* **2002**, *420*, 800−803.

(3) Colvin, V. L.; Schlamp, M. C.; Alivisatos, A. P. Light-emitting diodes made from cadmium selenide nanocrystals and a semiconducting polymer. *Nature* **1994**, *370*, 354−357.

(4) Sun, L.; Choi, J. J.; Stachnik, D.; Bartnik, A. C.; Hyun, B.; Malliaras, G. G.; Hanrath, T.; Wise, F. W. Bright infrared quantum-dot light-emitting diodes through inter-dot spacing control. *Nat. Nanotechnol.* **2012**, *7*, 369−373.

(5) Shirasaki, Y.; Supran, G. J.; Bawendi, M. G.; Bulovic, V. Emergence of colloidal quantum-dot light-emitting technologies. *Nat. Photonics* **2013**, *7*, 13−23.

(6) Lim, J.; Park, Y.; Wu, K.; Yun, H. J.; Klimov, V. I. Droop-Free Colloidal Quantum Dot Light-Emitting Diodes. *Nano Lett.* **2018**, *18*, 6645−6665.

(7) Supran, G. J.; Shirasaki, Y.; Song, K. W.; Caruge, J.; Kazlas, P. T.; Coe-sullivan, S.; Andrew, T. L.; Bawendi, M. G.; Bulovi, V. QLEDs for displays and solid-state lighting. *MRS Bull.* **2013**, *38*, 703−711.

(8) Cao, F.; Zhao, D.; Shen, P.; Wu, J.; Wang, H.; Wu, Q.; Wang, F.; Yang, X. High-Efficiency, Solution-Processed White Quantum Dot Light-Emitting Diodes with Serially Stacked Red/Green/Blue Units. *Adv. Opt. Mater.* **2018**, *6*, No. 1800652.

(9) Dai, X.; Deng, Y.; Peng, X.; Jin, Y. Quantum-Dot Light-Emitting Diodes for Large-Area Displays: Towards the Dawn of Commercialization. *Adv. Mater.* **2017**, *29*, No. 1607022.

(10) Klimov, V. I.; Mikhailovsky, A. A.; Xu, S.; Malko, A.; Hollingsworth, J. A.; Leatherdale, A. C.; Eisler, H.; Bawendi, M. G. Optical Gain and Stimulated Emission in Nanocrystal Quantum Dots. *Science* **2000**, *290*, 314−317.

(11) Yang, Z.; Pelton, M.; Fedin, I.; Talapin, D. V.; Waks, E. A room temperature continuous-wave nanolaser using colloidal quantum wells. *Nat. Commun.* **2017**, *8*, No. 143.

(12) Yun, C. S.; Javier, A.; Jennings, T.; Fisher, M.; Hira, S.; Peterson, S.; Hopkins, B.; Reich, N. O.; Strouse, G. F. Nanometal Surface Energy Transfer in Optical Rulers, Breaking the FRET Barrier. *J. Am. Chem. Soc.* **2005**, *127*, 3115.

(13) Medintz, I. L.; Clapp, A. R.; Mattoussi, H.; Goldman, E. R.; Fisher, B.; Mauro, J. M. Self-assembled nanoscale biosensors based on quantum dot FRET donors. *Nat. Mater.* **2003**, *2*, 630.

(14) Clapp, A. R.; Medintz, I. L.; Mauro, J. M.; Fisher, B. R.; Bawendi, M. G.; Mattoussi, H. Fluorescence Resonance Energy Transfer Between Quantum Dot Donors and Dye-Labeled Protein Acceptors. *J. Am. Chem. Soc.* **2004**, *126*, 301.

(15) Petryayeva, E.; Algar, W. R.; Medintz, I. L. Quantum Dots in Bioanalysis: A Review of Applications Across Various Platforms for Fluorescence Spectroscopy and Imaging. *Appl. Spectrosc.* **2013**, *67*, 215.

(16) Moroz, P.; Jin, Z.; Sugiyama, Y.; Lara, D.; Razgoniaeva, N.; Yang, M.; Kholmicheva, N.; Khon, D.; Mattoussi, H.; Zamkov, M. The Competition of Charge and Energy Transfer Processes in Donor-Acceptor Fluorescence Pairs: Calibrating the Spectroscopic Ruler. *ACS Nano* **2018**, *12*, 5657−5665.

(17) Beard, M. C.; Blackburn, J. L.; Johnson, J. C.; Rumbles, G. Status and Prognosis of Future Generation Photoconversion to Photovoltaics and Solar Fuels. *ACS Energy Lett.* **2016**, *1*, 344−347.

(18) Ko, D. K.; Maurano, A.; Suh, S. K.; Kim, D.; Hwang, G. W.; Grossman, J. C.; Bulovic, V.; Bawendi, M. G. Photovoltaic Performance of PbS Quantum Dots Treated with Metal Salts. *ACS Nano* **2016**, *10*, 3382−3388.

(19) Yang, Z.; Fan, J. Z.; Proppe, A. H.; Pelayo García de Arquer, F.; Rossouw, D.; Voznyy, O.; Lan, X.; Liu, M.; Walters, G.; Quintero-Bermudez, R.; Sun, B.; Hoogland, S.; Botton, G. A.; Kelley, S. O.;

Sargent, E. H. Mixed-Quantum-Dot Solar Cells. *Nat. Commun.* **2017**, *8*, No. 1325.
(20) Zamkov, M. Solar hydrogen generation: Exceeding 100% efficiency. *Nat. Energy* **2017**, *2*, No. 17072.
(21) Yan, Y.; Crisp, R. W.; Gu, J.; Chernomordik, B. D.; Pach, G. F.; Marshall, A. R.; Turner, J. A.; Beard, M. C. Multiple exciton generation for photoelectrochemical hydrogen evolution reactions with quantum yields exceeding 100%. *Nat. Energy* **2017**, *2*, No. 17052.
(22) Mongin, C.; Garakyaraghi, S.; Razgoniaeva, N.; Zamkov, M.; Castellano, F. N. Direct Observation of Triplet Energy Transfer from Semiconductor Nanocrystals. *Science* **2016**, *351*, 369−372.
(23) Peng, X.; Wickham, J.; Alivisatos, A. P. Kinetics of II-VI and III-V Colloidal Semiconductor Nanocrystal Growth: "Focusing" of Size Distributions. *J. Am. Chem. Soc.* **1998**, *120*, 5343−5344.
(24) Voznyy, O.; Levina, L.; Fan, J.; Askerka, M.; Jain, A.; Choi, M.; Ouellette, O.; Todorović, P.; Sagar, L.; Sargent, E. Machine Learning Accelerates Discovery of Optimal Colloidal Quantum Dot Synthesis. *ACS Nano* **2019**, *13*, 11122−11128.
(25) Talapin, D.; Rogach, A.; Kornowski, A.; Haase, M.; Weller, H. Highly Luminescent Monodisperse CdSe and CdSe/ZnS Nanocrystals Synthesized in a Hexadecylamine−Trioctylphosphine Oxide−Trioctylphospine Mixture. *Nano Lett.* **2001**, *1*, 207−211.
(26) Rogach, A.; Talapin, D.; Shevchenko, E.; Kornowski, A.; Haase, M.; Weller, H. Organization of Matter on Different Size Scales: Monodisperse Nanocrystals and Their Superstructures. *Adv. Funct. Mater.* **2002**, *12*, 653−664.
(27) Peng, X.; Manna, L.; Yang, W.; Wickham, J.; Scher, E.; Kadavanich, A.; Alivisatos, A. P. Shape Control of CdSe Nanocrystals. *Nature* **2000**, *404*, 59−61.
(28) Zhong, X.; Feng, Y.; Knoll, W.; Han, M. Alloyed $Zn_xCd_{1-x}S$ Nanocrystals with Highly Narrow Luminescence Spectral Width. *J. Am. Chem. Soc.* **2003**, *125*, 13559−13563.
(29) Li, J.; Wang, H.; Lin, L.; Fang, Q.; Peng, X. Quantitative Identification of Basic Growth Channels for Formation of Monodisperse Nanocrystals. *J. Am. Chem. Soc.* **2018**, *140*, 5474−5484.
(30) Zhou, J.; Pu, C.; Jiao, T.; Hou, X.; Peng, X. A Two-Step Synthetic Strategy toward Monodisperse Colloidal CdSe and CdSe/CdS Core/Shell Nanocrystals. *J. Am. Chem. Soc.* **2016**, *138*, 6475−6483.
(31) de Mello Donegá, C.; Hickey, S.; Wuister, S.; Vanmaekelbergh, D.; Meijerink, A. Single-Step Synthesis to Control the Photoluminescence Quantum Yield and Size Dispersion of CdSe Nanocrystals. *J. Phys. Chem. B* **2003**, *107*, 489−496.
(32) Gómez, D. E.; Embden, J.; Mulvaney, P. Spectral Diffusion of Single Semiconductor Nanocrystals: The Influence of the Dielectric Environment. *Appl. Phys. Lett.* **2006**, *88*, No. 154106.
(33) Razgoniaeva, N.; Carrillo, L.; Burchfield, D.; Moroz, P.; Adhikari, P.; Yadav, P.; Khon, D.; Zamkov, M. Colloidal Synthesis of Monodisperse Semiconductor Nanocrystals through the Saturated Ionic Layer Adsorption. *Chem. Mater.* **2016**, *28*, 2823−2833.
(34) Tan, R.; Yuan, Y.; Nagaoka, Y.; Eggert, D.; Wang, X.; Thota, S.; Guo, P.; Yang, H.; Zhao, J.; Chen, O. Monodisperse Hexagonal Pyramidal and Bipyramidal Wurtzite CdSe-CdS Core−Shell Nanocrystals. *Chem. Mater.* **2017**, *29*, 4097−4108.
(35) Flamee, S.; Cirillo, M.; Abe, S.; Nolf, K.; Gomes, R.; Aubert, T.; Hens, Z. Fast, High Yield, and High Solid Loading Synthesis of Metal Selenide Nanocrystals. *Chem. Mater.* **2013**, *25*, 2476−2483.
(36) Park, J.; Joo, J.; Kwon, S. G.; Jang, Y.; Hyeon, T. Synthesis of Monodisperse Spherical Nanocrystals. *Angew. Chem., Int. Ed.* **2007**, *46*, 4630−4660.
(37) Razgoniaeva, N.; Carrillo, L.; Burchfield, D.; Moroz, P.; Adhikari, P.; Yadav, P.; Khon, D.; Zamkov, M. Colloidal Synthesis of Monodisperse Semiconductor Nanocrystals through the Saturated Ionic Layer Adsorption. *Chem. Mater.* **2016**, *28*, 2823−2833.
(38) Dai, Q.; Wang, Y.; Li, X.; Zhang, Y.; Pellegrino, D. J.; Zhao, M.; Zou, B.; Seo, J.; Wang, Y.; Yu, W. W. Size-Dependent Composition and Molar Extinction Coefficient of PbSe Semiconductor Nanocrystals. *ACS Nano* **2009**, *3*, 1518−1524.
(39) Morris-Cohen, A. J.; Frederick, M. T.; Lilly, G. D.; Mcarthur, E. A.; Weiss, E. A. Organic Surfactant Controlled Composition of the Surfaces of CdSe Quantum Dots. *J. Phys. Chem. Lett.* **2010**, *1*, 1078−1081.
(40) Smith, D. K.; Luther, J. M.; Semonin, O. E.; Nozik, A. J.; Beard, M. C. Tuning the Synthesis of Ternary Lead Chalcogenide Quantum Dots by Balancing Precursor Reactivity. *ACS Nano* **2011**, *5*, 183−190.
(41) Chen, O.; Yang, Y. A.; Wang, T.; Wu, H. M.; Niu, C. G.; Yang, J. H.; Cao, Y. C. Surface-Functionalization-Dependent Optical Properties of II-VI Semiconductor Nanocrystals. *J. Am. Chem. Soc.* **2011**, *133*, 17504−17512.
(42) Hassinen, A.; Moreels, I.; De Nolf, K.; Smet, P. F.; Martins, J. C.; Hens, Z. Short-Chain Alcohols Strip X-Type Ligands and Quench the Luminescence of PbSe and CdSe Quantum Dots, Acetonitrile Does Not. *J. Am. Chem. Soc.* **2012**, *134*, 20705−20712.
(43) Munro, A. M.; Ginger, D. S. Photoluminescence Quenching of Single CdSe Nanocrystals by Ligand Adsorption. *Nano Lett.* **2008**, *8*, 2585−2590.
(44) Sugimoto, T. Preparation of Monodispersed Colloidal Particles. *Adv. Colloid Interface Sci.* **1987**, *28*, 65−108.
(45) Lifshitz, I.; Slyozov, V. J. The Kinetics of Precipitation from Supersaturated Solid Solutions. *J. Phys. Chem. Solids* **1961**, *19*, 35−50.
(46) Penn, R. L.; Banfield, J. F. Imperfect Oriented Attachment: Dislocation Generation in Defect-Free Nanocrystals. *Science* **1998**, *281*, 969−971.
(47) Wang, F.; Richards, V. N.; Shields, S. P.; Buhro, W. E. Kinetics and Mechanisms of Aggregative Nanocrystal Growth. *Chem. Mater.* **2014**, *26*, 5−21.
(48) Kumar, S.; Davis, T. M.; Ramanan, H.; Penn, R. L.; Tsapatsis, M. Aggregative growth of silicalite-1. *J. Phys. Chem. B* **2007**, *111*, 3398−3403.
(49) Yu, K.; Ouyang, J.; Leek, D. M. In-situ observation of nucleation and growth of PbSe magic-sized nanoclusters and regular nanocrystals. *Small* **2011**, *7*, 2250−2262.
(50) Razgoniaeva, N.; Yang, M.; Garrett, P.; Kholmicheva, N.; Moroz, P.; Eckard, H.; Royo Romero, L.; Porotnikov, D.; Khon, D.; Zamkov, M. Just Add Ligands: Self-Sustained Size Focusing of Colloidal Semiconductor Nanocrystals. *Chem. Mater.* **2018**, *30*, 1391−1398.
(51) Cheng, T.; Marin, R.; Skripka, A.; Vetrone, F. Small and Bright Lithium-Based Upconverting Nanoparticles. *J. Am. Chem. Soc.* **2018**, *140*, 12890−12899.
(52) Yu, L.; You, H.; Zhang, Q.; Zhang, L.; Fang, J. Digestive ripening mechanism investigation in a classical Lee−Meisel method based on in situ UV−vis spectra. *CrystEngComm* **2019**, *21*, 1529−1533.
(53) Kim, M.; Jeong, J.; Choi, Y.; Park, J.; Park, E.; Cheon, C.; Kim, N.; Min, B. K.; Kim, W. Synthesis of V-doped In_2O_3 Nanocrystals via Digestive-Ripening Process and Their Electrocatalytic Properties in CO_2 Reduction Reaction. *ACS Appl. Mater. Interfaces* **2020**, *12*, 11890−11897.
(54) Cassidy, J.; Zamkov, M. Nanoshell Quantum Dots: Quantum Confinement Beyond the Exciton Bohr Radius. *J. Chem. Phys.* **2020**, *152*, No. 110902.
(55) Kholmicheva, N.; Yang, M.; Moroz, P.; Eckard, H.; Vore, A.; Cassidy, J.; Pushina, M.; Boddy, A.; Porotnikov, D.; Anzenbacher, P.; Zamkov, M. Ion-Mediated Ligand Exchange and Size Focusing of Semiconductor Nanocrystals in Ligand-Saturated Solutions. *J. Phys. Chem. C* **2018**, *122*, 23623−23630.
(56) Shimpi, J. R.; Sidhaye, D. S.; Prasad, B. L. V. Digestive Ripening: A Fine Chemical Machining Process on the Nanoscale. *Langmuir* **2017**, *33*, 9491−9507.
(57) Zheng, H.; Smith, R. K.; Jun, Y. W.; Kisielowski, C.; Dahmen, U.; Alivisatos, A. P. Observation of Single Colloidal Platinum Nanocrystal Growth Trajectories. *Science* **2009**, *324*, 1309−1312.
(58) Yuk, J. M.; Park, J.; Ercius, P.; Kim, K.; Hellebusch, D. J.; Crommie, M. F.; Lee, J. Y.; Zettl, A.; Alivisatos, A. P. High-Resolution TEM of Colloidal Nanocrystal Growth Using Graphene Liquid Cells. *Science* **2012**, *336*, 61−64.

https://dx.doi.org/10.1021/acs.chemmater.0c02874
Chem. Mater. 2020, 32, 7524−7534

(59) Wang, F.; Richards, V. N.; Shields, S. P.; Buhro, W. E. Kinetics and Mechanisms of Aggregative Nanocrystal Growth. *Chem. Mater.* **2014**, *26*, 5−21.
(60) Polte, J.; Ahner, T. T.; Delissen, F.; Sokolov, S.; Emmerling, F.; Thunemann, A. F.; Kraehnert, R. Mechanism of Gold Nanoparticle Formation in the Classical Citrate Synthesis Method Derived from Coupled In Situ XANES and SAXS Evaluation. *J. Am. Chem. Soc.* **2010**, *132*, 1296−1301.
(61) Penn, R. L.; Banfield, J. F. Imperfect Oriented Attachment: Dislocation Generation in Defect-Free Nanocrystals. *Science* **1998**, *281*, 969−971.
(62) Tang, Z. Y.; Kotov, N. A.; Giersig, M. Spontaneous Organization of Single CdTe Nanoparticles into Luminescent Nanowires. *Science* **2002**, *297*, 237−240.
(63) Ithurria, S.; Dubertret, B. Quasi 2D colloidal CdSe platelets with thicknesses controlled at the atomic level. *J. Am. Chem. Soc.* **2008**, *130*, 16504−16505.
(64) Schliehe, C.; Juarez, B. H.; Pelletier, M.; Jander, S.; Greshnykh, D.; Nagel, M.; Meyer, A.; Foerster, S.; Kornowski, A.; Klinke, C.; Weller, H. Ultrathin PbS Sheets by Two-Dimensional Oriented Attachment. *Science* **2010**, *329*, 550−553.
(65) Joo, J.; Son, J.; Kwon, S.; Yu, S.; Hyeon, T. Low-temperature solution-phase synthesis of quantum well structured CdSe nanoribbons. *J. Am. Chem. Soc.* **2006**, *128*, 5632−5633.
(66) Son, J. S.; Wen, X. D.; Joo, J.; Chae, J.; Baek, S.; Park, K.; Kim, J. H.; An, K.; Yu, J. H.; Kwon, S. G.; Choi, S. H.; Wang, Z.; Kim, Y. W.; Kuk, Y.; Hoffmann, R.; Hyeon, T. Large-Scale Soft Colloidal Template Synthesis of 1.4 nm Thick CdSe Nanosheets. *Angew. Chem., Int. Ed.* **2009**, *48*, 6861−6864.
(67) Tang, Z. Y.; Zhang, Z. L.; Wang, Y.; Glotzer, S. C.; Kotov, N. A. Self-assembly of CdTe nanocrystals into free-floating sheets. *Science* **2006**, *314*, 274−278.
(68) Ostwald, W. On the Assumed Isomerism of Red and Yellow Mercury Oxide and the Surface-Tension of Solid Bodies. *Z. Phys. Chem.* **1900**, *34*, 495−503.
(69) Hendriks, E. M.; Ernst, W. H. Exactly Soluble Addition and Condensation Models in Coagulation Kinetics. *J. Colloid Interface Sci.* **1984**, *97*, 176−194.
(70) Lifshitz, I.; Slyozov, V. J. The Kinetics of Precipitation from Supersaturated Solid Solutions. *J. Phys. Chem. Solids* **1961**, *19*, 35−50.
(71) Karatutlu, A.; Barhoum, A.; Sapelkin, A. Theories of nanoparticle and nanostructure formation in liquid phase. In *Emerging Applications of Nanoparticles and Architecture Nanostructures*; Elsevier Inc., 2018; pp 597−619.
(72) Liu, H.; Owen, J. S.; Alivisatos, A. P. Mechanistic Study of Precursor Evolution in Colloidal Group II-VI Semiconductor Nanocrystal Synthesis. *J. Am. Chem. Soc.* **2007**, *129*, 305−312.
(73) Rempel, J. Y.; Bawendi, M. G.; Jensen, K. F. Insights into the kinetics of semiconductor nanocrystal nucleation and growth. *J. Am. Chem. Soc.* **2009**, *131*, 4479−4489.
(74) Zhuang, Z.; Peng, Q.; Li, Y. Controlled synthesis of semiconductor nanostructures in the liquid phase. *Chem. Soc. Rev.* **2011**, *40*, 5492−5513.
(75) García-Rodríguez, R.; Hendricks, M. P.; Cossairt, B. M.; Liu, H.; Owen, J. S. Conversion reactions of cadmium chalcogenide nanocrystal precursors. *Chem. Mater.* **2013**, *25*, 1233−1249.
(76) Thanh, N. T.; Maclean, N.; Mahiddine, S. Mechanisms of nucleation and growth of nanoparticles in solution. *Chem. Rev.* **2014**, *114*, 7610−7630.
(77) Abe, S.; Čapek, R. K.; De Geyter, B.; Hens, Z. Tuning the Postfocused Size of Colloidal Nanocrystals by the Reaction Rate: From Theory to Application. *ACS Nano* **2012**, *6*, 42−53.
(78) Zhang, Q.; Liu, S.; Yu, S. Recent Advances in Oriented Attachment Growth and Synthesis of Functional Materials: Concept, Evidence, Mechanism, and Future. *J. Mater. Chem.* **2009**, *19*, 191−207.
(79) Jun, Y. W.; Casula, M. F.; Sim, J. H.; Kim, S. Y.; Cheon, J.; Alivisatos, A. P. Surfactant-assisted elimination of a high energy facet as a means of controlling the shapes of TiO_2 nanocrystals. *J. Am. Chem. Soc.* **2003**, *125*, 15981−15985.
(80) Cho, K. S.; Talapin, D. V.; Gaschler, W.; Murray, C. B. Designing PbSe nanowires and nanorings through oriented attachment of nanoparticles. *J. Am. Chem. Soc.* **2005**, *127*, 7140−7147.
(81) Liu, Y. H.; Wang, F. D.; Wang, Y. Y.; Gibbons, P. C.; Buhro, W. E. Lamellar Assembly of Cadmium Selenide Nanoclusters into Quantum Belts. *J. Am. Chem. Soc.* **2011**, *133*, 17005−17013.
(82) Lhuillier, E.; Pedetti, S.; Ithurria, S.; Nadal, B.; Heuclin, H.; Dubertret, B. Two-Dimensional Colloidal Metal Chalcogenides Semiconductors: Synthesis, Spectroscopy, and Applications. *Acc. Chem. Res.* **2015**, *48*, 22−30.
(83) Schliehe, C.; Juarez, B. H.; Pelletier, M.; Jander, S.; Greshnykh, D.; Nagel, M.; Meyer, A.; Foerster, S.; Kornowski, A.; Klinke, C.; Weller, H. Ultrathin PbS Sheets by Two-Dimensional Oriented Attachment. *Science* **2010**, *329*, 550−553.
(84) Penn, R. L. Imperfect Oriented Attachment: Dislocation Generation in Defect-Free Nanocrystals. *Science* **1998**, *281*, 969−971.
(85) Moldovan, D.; Yamakov, V.; Wolf, D.; Phillpot, S. R. Scaling behavior of grain-rotation-induced grain growth. *Phys. Rev. Lett.* **2002**, *89*, No. 206101.
(86) Zhang, J.; Huang, F.; Lin, Z. Progress of nanocrystalline growth kinetics based on oriented attachment. *Nanoscale* **2010**, *2*, 18−34.
(87) Peng, X.; Wickham, J.; Alivisatos, A. P. Kinetics of II-VI and III-V colloidal semiconductor nanocrystal growth: "focusing" of size distributions. *J. Am. Chem. Soc.* **1998**, *120*, 5343−5344.
(88) Zhang, J.; Wang, Y. H.; Zheng, J. S.; Huang, F.; Chen, D. G.; Lan, Y. Z.; Ren, G. Q.; Lin, Z.; Wang, C. Oriented attachment kinetics for ligand capped nanocrystals: Coarsening of thiol-PbS nanoparticles. *J. Phys. Chem. B* **2007**, *111*, 1449−1454.
(89) Privman, V.; Goia, D. V.; Park, J.; Matijeviæ, E. Mechanism of Formation of Monodispersed Colloids by Aggregation of Nanosize Precursors. *J. Colloid Interface Sci.* **1999**, *213*, 36−45.
(90) Park, J.; Privman, V.; Matijeviæ, E. Model of Formation of Monodispersed Colloids. *J. Phys. Chem. B* **2001**, *105*, 11630−11635.
(91) Carbone, L.; Nobile, C.; De Giorgi, M.; Della Salla, F.; Morello, G.; Pompa, P.; Hytch, M.; Snoeck, E.; Fiore, A.; Franchini, I. R.; Nadasan, M.; Silvestre, A. F.; Chiodo, L.; Kudera, S.; Cingolani, R.; Krahne, R.; Manna, L. Synthesis and Micrometer-Scale Assembly of Colloidal CdSe/CdS Nanorods Prepared by a Seeded Growth Approach. *Nano Lett.* **2007**, *7*, 2942−2950.
(92) Peng, Z. A.; Peng, X. G. Nearly Monodisperse and Shape-Controlled CdSe Nanocrystals via Alternative Routes: Nucleation and Growth. *J. Am. Chem. Soc.* **2002**, *124*, 3343−3353.
(93) Bogush, G. H.; Zukoski, C. F. Uniform silica particle precipitation: An aggregative growth model. *J. Colloid Interface Sci.* **1991**, *142*, 19−34.
(94) Van Hyning, D. L.; Klemperer, W. G.; Zukoski, C. F. Silver Nanoparticle Formation: Predictions and Verification of the Aggregative Growth Model. *Langmuir* **2001**, *17*, 3128−3135.
(95) Busby, E.; Anderson, N. C.; Owen, J. S.; Sfeir, M. Y. Effect of Surface Stoichiometry on Blinking and Hole Trapping Dynamics in CdSe Nanocrystals. *J. Phys. Chem. C* **2015**, *119*, 27797−27803.
(96) Houtepen, A. J.; Hens, H.; Owen, J. S.; Infante, I. On the Origin of Surface Traps in Colloidal II−VI Semiconductor Nanocrystals. *Chem. Mater.* **2017**, *29*, 752−761.
(97) Smith, D. K.; Luther, J. M.; Semonin, O. E.; Nozik, A. J.; Beard, M. C. Tuning the Synthesis of Ternary Lead Chalcogenide Quantum Dots by Balancing Precursor Reactivity. *ACS Nano* **2011**, *5*, 183−190.
(98) Peng, X. G.; Wickham, J.; Alivisatos, A. P. Kinetics of II-VI and III-V Colloidal Semiconductor Nanocrystal Growth: "Focusing" of Size Distributions. *J. Am. Chem. Soc.* **1998**, *120*, 5343−5344.
(99) Anderson, N. C.; Owen, J. S. Soluble, Chloride-Terminated CdSe Nanocrystals: Ligand Exchange Monitored by ^{1}H and ^{31}P NMR Spectroscopy. *Chem. Mater.* **2013**, *25*, 69−76.
(100) Ji, X.; Copenhaver, D.; Sichmeller, C.; Peng, X. Ligand Bonding and Dynamics on Colloidal Nanocrystals at Room Temperature: The Case of Alkylamines on CdSe Nanocrystals. *J. Am. Chem. Soc.* **2008**, *130*, 5726−5735.

https://dx.doi.org/10.1021/acs.chemmater.0c02874
Chem. Mater. 2020, 32, 7524−7534

(101) Saniepay, M.; Mi, C.; Liu, Z.; Abel, E. P.; Beaulac, R. Insights into the Structural Complexity of Colloidal CdSe Nanocrystal Surfaces: Correlating the Efficiency of Nonradiative Excited-State Processes to Specific Defects. *J. Am. Chem. Soc.* **2018**, *140*, 1725−1736.
(102) Kholmicheva, N.; Yang, M.; Moroz, P.; Eckard, H.; Vore, A.; Cassidy, J.; Pushina, M.; Boddy, A.; Porotnikov, D.; Anzenbacher, P.; Zamkov, M. Ion-Mediated Ligand Exchange and Size-Focusing of Semiconductor Nanocrystals in Ligand-Saturated Solutions. *J. Phys. Chem. C* **2018**, *122*, 23623−23630.
(103) Talapin, D. V.; Rogach, A. L.; Kornowski, A.; Haase, M.; Weller, H. Highly Luminescent Monodisperse CdSe and CdSe/ZnS Nanocrystals Synthesized in a Hexadecylamine-Trioctylphosphine Oxide-Trioctylphospine Mixture. *Nano Lett.* **2001**, *1*, 207−211.
(104) Brown, P. R.; Kim, D.; Lunt, R. R.; Zhao, N.; Bawendi, M. G.; Grossman, J. C.; Bulovic′, V. Energy Level Modification in Lead Sulfide Quantum Dot Thin Films through Ligand Exchange. *ACS Nano* **2014**, *8*, 5863−5872.
(105) Mack, T.; Jethi, L.; Kambhampati, P. Temperature Dependence of Emission Line Widths from Semiconductor Nanocrystals Reveals Vibronic Contributions to Line Broadening Processes. *J. Phys. Chem. C.* **2017**, *121*, 28537−28545.
(106) Chen, O.; Zhao, J.; Chauhan, V.; Cui, J.; Wong, C.; Harris, D.; Wei, H.; Han, H.; Fukumura, D.; Jain, R.; Bawendi, M. Compact High-Quality CdSe−CdS Core−Shell Nanocrystals with Narrow Emission Linewidths and Suppressed Blinking. *Nat. Mater.* **2013**, *12*, 445−451.
(107) Cui, J.; Beyler, A.; Coropceanu, I.; Cleary, L.; Avila, T.; Chen, Y.; Cordero, J.; Heathcote, S.; Harris, D.; Chen, O.; Cao, J.; Bawendi, M. Evolution of the Single-Nanocrystal Photoluminescence Linewidth with Size and Shell: Implications for Exciton−Phonon Coupling and the Optimization of Spectral Linewidths. *Nano Lett.* **2016**, *16*, 289−296.
(108) Cui, J.; Beyler, A. P.; Coropceanu, I.; Cleary, L.; Avila, T. R.; Chen, Y.; Cordero, J. M.; Heathcote, S. L.; Harris, D. K.; Chen, O.; Cao, J.; Bawendi, M. G. Evolution of the single-nanocrystal photoluminescence linewidth with size and shell: Implications for exciton−phonon coupling and the optimization of spectral linewidths. *Nano Lett.* **2016**, *16*, 289−296.
(109) Zhou, J.; Pu, C.; Jiao, T.; Hou, X.; Peng, X. A Two-Step Synthetic Strategy toward Monodisperse Colloidal CdSe and CdSe/CdS Core/ Shell Nanocrystals. *J. Am. Chem. Soc.* **2016**, *138*, 6475−6483.
(110) Talapin, D. V.; Lee, J. S.; Kovalenko, M. V.; Shevchenko, E. V. Prospects of Colloidal Nanocrystals for Electronic and Optoelectronic Applications. *Chem. Rev.* **2010**, *110*, 389−458.
(111) Qu, L.; Peng, X. Control of photoluminescence properties of CdSe nanocrystals in growth. *J. Am. Chem. Soc.* **2002**, *124*, 2049.
(112) Privman, V.; Goia, D. V.; Park, J.; Matijevic, E. J. Mechanism of Formation of Monodispersed Colloids by Aggregation of Nanosize Precursors. *J. Colloid Interface Sci.* **1999**, *213*, 36−45.
(113) Smoluchowski, M. Drei Vortrage uber Diffusion, Brownsche Bewegung und Koagulation von Kolloidteilchen. *Phys. Z.* **1916**, *17*, 557−585.
(114) Meakin, P. Formation of fractal clusters and networks by irreversible diffusion-limited aggregation. *Phys. Rev. Lett.* **1983**, *51*, 1119−1122.
(115) Weitz, D. A.; Huang, J. S.; Lin, M. Y.; Sung, J. Limits of the fractal dimension for irreversible kinetic aggregation of gold colloids. *Phys. Rev. Lett.* **1985**, *54*, 1416−1419.
(116) Brilliantov, N. V.; Albers, N.; Spahn, F.; Poschel, T. Collision dynamics of granular particles with adhesion. *Phys. Rev. E* **2007**, *76*, No. 051302.
(117) Pawar, A. B.; Caggioni, M.; Hartel, R. W.; Spicer, P. T. Arrested coalescence of viscoelastic droplets with internal microstructure. *Faraday Discuss.* **2012**, *158*, 341−350.
(118) Varshni, Y. P. Temperature dependence of the elastic constants. *Phys. Rev. B* **1970**, *2*, 3952−3958.
(119) Zhang, J.; Lin, Z.; Lan, Y. Z.; Ren, G. Q.; Chen, D. G.; Huang, F.; Hong, M. C. A multistep oriented attachment kinetics: Coarsening of ZnS nanoparticle in concentrated NaOH. *J. Am. Chem. Soc.* **2006**, *128*, 12981−12987.
(120) Yu, W. W.; Peng, X. Formation of High-Quality CdS and Other II−VI Semiconductor Nanocrystals in Noncoordinating Solvents: Tunable Reactivity of Monomers. *Angew. Chem., Int. Ed.* **2002**, *41*, 2368−2371.
(121) Carbone, L.; Nobile, C.; De Giorgi, M.; Della Salla, F.; Morello, G.; Pompa, P.; Hytch, M.; Snoeck, E.; Fiore, A.; Franchini, I. R.; Nadasan, M.; Silvestre, A. F.; Chiodo, L.; Kudera, S.; Cingolani, R.; Krahne, R.; Manna, L. Synthesis and Micrometer-Scale Assembly of Colloidal CdSe/CdS Nanorods Prepared by a Seeded Growth Approach. *Nano Lett.* **2007**, *7*, 2942−2950.
(122) Yu, W. W.; Qu, L. H.; Guo, W. Z.; Peng, X. G. Experimental determination of the extinction coefficient of CdTe, CdSe, and CdS nanocrystals. *Chem. Mater.* **2003**, *15*, 2854−2860.

https://dx.doi.org/10.1021/acs.chemmater.0c02874
Chem. Mater. 2020, 32, 7524−7534